International Journal of Solids and Structures 49 (2012) 2239–2253

Contents lists available at SciVerse ScienceDirect

International Journal of Solids and Structures

journal homepage: www.elsevier.com/locate/ijsolstr

Planar isotropic structures with negative Poisson's ratio

Igor Shufrin [a,b], Elena Pasternak [a], Arcady V. Dyskin [b,*]

[a] School of Mechanical and Chemical Engineering, The University of Western Australia, 35 Stirling Highway, Crawley, WA 6009, Australia
[b] School of Civil and Resource Engineering, The University of Western Australia, 35 Stirling Highway, Crawley, WA 6009, Australia

ARTICLE INFO

Article history:
Received 28 June 2011
Received in revised form 27 February 2012
Available online 26 April 2012

Keywords:
Auxetic isotropic structures
Homogenisation
Cosserat continuum
Reinforcing core

ABSTRACT

A new design principle is suggested for constructing auxetic structures – the structures that exhibit negative Poisson's ratio (NPR) at macroscopic level. We propose 2D assemblies of identical units made of a flexible frame with a sufficiently rigid reinforcing core at the centre. The core increases the frame resistance to the tangential movement thus ensuring high shear stiffness, whereas the normal stiffness is low being controlled by the local bending response of the frame. The structures considered have hexagonal symmetry, which delivers macroscopically isotropic elastic properties in the plane perpendicular to the axis of the symmetry. We determine the macroscopic Poisson's ratio as a ratio of corresponding relative displacements computed using the direct microstructural approach. It is demonstrated that the proposed design can produce a macroscopically isotropic system with NPR close to the lower bound of −1. We also developed a 2D elastic Cosserat continuum model, which represents the microstructure as a regular assembly of rigid particles connected by elastic springs. The comparison of values of NPRs computed using both structural models and the continuum approach shows that the continuum model gives a healthy balance between the simplicity and accuracy and can be used as a simple tool for design of auxetics.

1. Introduction

Negative Poisson's ratio (NPR) materials contract laterally when compressed longitudinally and expand in the transverse direction under axial tension. Although being theoretically predicted a long time ago, materials with NPR or so-called auxetic materials (Evans et al., 1991) have mostly attracted attention during the last three decades. Due to their unique behaviour, auxetic materials are able to provide high shear to bulk modulus ratio and, in some cases, an increase in fracture toughness (e.g., Choi and Lakes, 1996; Donoghue et al., 2009) and a reduction in thermal stresses (Pasternak and Dyskin, 2012). In addition, they can be useful in applications where compaction under impact is required and where high indentation resistance is essential (Alderson and Alderson, 2007; Yang et al., 2004). A wide range of auxetic materials have been theoretically predicted and some prototypes manufactured. These include, but are not limited to, cellular solids and foams (Attard and Grima, 2011; Bianchi et al., 2011; Chan and Evans, 1997; Choi and Lakes, 1992a,b; Evans et al., 1991; Gaspar et al., 2005; Grima et al., 2006; Kolpakov, 1985; Lakes, 1987; Scarpa et al., 2005; Smith et al., 2000), microporous polymers (Caddock and Evans, 1989; Alderson and Evans, 1992), particulate composites (Wei and Edwards, 1998), fibre reinforced (Alderson et al., 2005; Coenen and Alderson, 2011; Jayanty et al., 2011; Zhang et al., 1999) and laminated composites (Lim, 2009; Lim and Rajendra Acharya, 2011; Shokrieh and Assadi, 2011), auxetic yarns (Miller et al., 2009; Wright et al., 2010), and nanocomposites (Hall et al., 2008; Scarpa et al., 2010).

The design of these materials has been based on microstructures with macroscopic (structural) NPR, where a fundamental structural unit unfolds when stretched and folds back when compressed (Blumenfeld, 2005). The most cited example of these units is the re-entrant honeycomb, which was proposed as a basic module of auxetic foams and cellular solids by Lakes (1987) and Evans et al. (1991), and then by others (Alderson and Alderson, 2007; Liu and Hu, 2010; Michelis and Spitas, 2010; Lira et al., 2010; Miller et al., 2011). Deforming by bending of the cell walls, the re-entrant honeycomb exhibits NPR on the cell level, which in turn produces the macroscopic auxetic effect. However, in contrast with a conventional honeycomb, the re-entrant honeycomb network does not have the hexagonal symmetry, which in turn leads to the loss of isotropy (hexagonal symmetry leads to elastic isotropy in 2D, (Landau and Lifshitz, 1986)). It is important to recall here that for isotropic materials the thermodynamics restricts the Poisson's ratio to be in the range of −1 to 0.5, while in anisotropic media the range is wider and depends upon the type of anisotropy (e.g., Tshernykh, 1988). Furthermore, the advantages of auxetic materials are usually discussed and analysed in isotropic context.

Another approach to produce an auxetic microstructure is based on constructing networks of rigid blocks connected by

* Corresponding author.
E-mail address: arcady@civil.uwa.edu.au (A.V. Dyskin).

0020-7683/$ - see front matter © 2012 Elsevier Ltd. All rights reserved.
http://dx.doi.org/10.1016/j.ijsolstr.2012.04.022

flexible links. This scheme has been employed for simulating the natural auxetics using networks of units built from 2D and 3D rigid rotating blocks of different shapes by Alderson and Evans (2001), Attard et al. (2009a,b), Grima et al. (2005, 2009, 2010) and Williams et al. (2007). Microstructures of auxetic polymers have also been modelled as networks of rectangular nodules connected by fibrils (Alderson and Evans, 1997; Evans and Caddock, 1989; Gaspar et al., 2011). Also a structure consisting of rigid blocks with interlocking (lego-type) connections shows an auxetic effect (Bathurst and Rothenburg, 1988; Ravirala et al., 2007).

The length scale of microstructures proposed as building blocks for auxetic materials varies significantly from large engineering structures down to molecular and nano-auxetic composites (Evans and Alderson, 2000). This is not surprising since the Poisson's ratio is a property of elastic continuum which is scale independent.

Some authors looked for elementary auxetic structures at the molecular level (e.g., Evans et al., 1991). Vasiliev et al. (2002) suggested that molecular rotations and anisotropy are essential for a description of auxetic performance. They developed an anisotropic model of a crystal consisting of elastically restrained rigid particles, which produces NPR. However, using Monte–Carlo simulations Wojciechowski (2003) showed that isotropic auxeticity can be obtained without molecular rotations. Wojciechowski and co-authors investigated various molecular configurations of hard and soft cyclic multimers (Kowalik and Wojciechowski, 2008; Narojczyk et al., 2008; Narojczyk and Wojciechowski, 2008, 2010; Tretiakov and Wojciechowski, 2007; Wojciechowski, 1989), which produce thermodynamically stable auxetic phases. We note that these results were obtained from computer simulations; a real molecular prototype is yet to be fabricated. Furthermore, the aforementioned structures are not isotropic.

The main objective of this study is to develop 2D auxetic structures exhibiting isotropic behaviour at the macrolevel. To this end we use an approach based on micromechanical models of granulate materials developed in Bathurst and Rothenburg (1988) using the classical theory of elasticity and Pasternak and Mühlhaus (2001), Pasternak et al. (2004) and Pasternak and Mühlhaus (2005) using the Cosserat continuum. In these models, mechanical properties of a granulate material are derived as a function of contact interactions between the particles, which are represented by normal and tangential linear springs and, in the case of the Cosserat model, by additional rotational springs. It has been shown that the ratio between stiffnesses of the tangential and normal springs governs the macroscopic Poisson's ratio. Rothenburg et al. (1991) showed that the ratio of shear to normal stiffnesses of the microstructural cells can be used to interpret the auxetic behaviour of non-granular materials as well. These principles of the design of auxetic materials were implemented by Pasternak and Dyskin (2008a,b), Pasternak et al. (2010), and Pasternak and Dyskin (2012), in 2D and 3D, and by Shufrin et al. (2010), and Gaspar (2010) in 2D. In particular, auxetic ball-rod structures and structures made of thin wall spheres, as well as a matrix with cracks with suppressed shear displacement discontinuity were considered by Pasternak and Dyskin (2008a,b, 2012). These authors also suggested hybrid materials made of an isotropic matrix with spherical inclusions having Poisson's ratios of different signs and found the effect of gigantic stiffening produced by conventional inclusions in the auxetic matrix. Pasternak and Dyskin (2012) also studied generic mechanical properties (fracture and thermal) of auxetic materials as well as the wave propagation and energy dissipation in viscoelastic auxetics. It was concluded that there is no coupling between NPR and the enhanced fracture toughness or damping; rather some microstructures which macroscopically exhibit negative Poisson's ratio may independently have increased fracture toughness or energy dissipation as well.

Here we extend these ideas and introduce novel auxetic microstructures with hexagonal symmetry that macroscopically exhibit isotropic elastic properties in the symmetry plane (in 3D these structures are transverse-isotropic). We analyse these systems numerically using the homogenisation procedure and the direct structural analysis. We use the continuum micromechanical model, which has originally been developed for an assembly of rigid particles, to describe interactions between elastic elements of the assembly. We discuss various aspects of performance of the proposed structures and show that these isotropic microstructures are able to provide the Poisson's ratio close to the lower bound of -1.

2. Negative Poisson's ratio in a regular planar assembly

Basic principles for the design of isotropic microstructures of auxetic materials are established using a micromechanical approach of homogenisation of energy of interactions between particles in a regular arrangement. We consider a planar hexagonal assembly of circular particles (discs) elastically bonded to each other. This structure has a six-order axis of symmetry. In 3D this macroscopically forms a transverse isotropic elastic material. However, in the plane of the layer the macroscopic material is isotropic (e.g., Landau and Lifshitz, 1986). Consequently following the homogenisation procedure of Pasternak and Mühlhaus (2005) developed for 3D Cosserat continuum, we derive a 2D Cosserat continuum model for this planar assembly. We show that the negative values of the Poisson's ratio can be obtained under certain stiffness parameters of the bonds.

In this regular close-packed hexagonal assembly of identical discs the interaction between two neighbouring discs is represented as a set of linear springs, namely: two translational springs normal and tangential to the contact between the discs and a rotational spring. The normal and tangential (shear) spring stiffnesses, k_n and k_s are defined as the corresponding contact forces produced by unit relative displacements, while the rotational spring stiffness k_ϕ is the contact moment produced by a unit relative rotation. Defining a potential of the contact springs and then applying the method of homogenisation by differential expansion as in Pasternak and Mühlhaus (2005), the constitutive relations of the equivalent 2D Cosserat continuum are recovered as follows (see Appendix A for details).

$$\sigma_{11} = \frac{\sqrt{3}}{4h}((3k_n + k_s)\gamma_{11} + (k_n - k_s)\gamma_{22}) \tag{1.1}$$

$$\sigma_{12} = \frac{\sqrt{3}}{4h}((k_n + 3k_s)\gamma_{12} + (k_n - k_s)\gamma_{21}) \tag{1.2}$$

$$\sigma_{21} = \frac{\sqrt{3}}{4h}((k_n - k_s)\gamma_{12} + (k_n + 3k_s)\gamma_{21}) \tag{1.3}$$

$$\sigma_{22} = \frac{\sqrt{3}}{4h}((k_n - k_s)\gamma_{11} + (3k_n + k_s)\gamma_{22}) \tag{1.4}$$

$$\mu_{13} = \frac{\sqrt{3}}{h}k_\phi\kappa_{13} \tag{1.5}$$

$$\mu_{23} = \frac{\sqrt{3}}{h}k_\phi\kappa_{23} \tag{1.6}$$

Here, σ_{ij} and μ_{ij} are the (non-symmetric) stress and moment stress respectively, γ_{ij} and κ_{ij} are the Cosserat strain and curvature, and h is the thickness of the assembly.

We now compare these relationships with the constitutive equations for isotropic Cosserat continuum, which in the plane stress state read

$$\sigma_{11} = 2\mu\frac{2(\mu+\lambda)}{2\mu+\lambda}\gamma_{11} + 2\mu\frac{\lambda}{2\mu+\lambda}\gamma_{22} \tag{2.1}$$

$$\sigma_{12} = (\mu-\alpha)\gamma_{21} + (\mu+\alpha)\gamma_{12} \tag{2.2}$$

$$\sigma_{21} = (\mu+\alpha)\gamma_{21} + (\mu-\alpha)\gamma_{12} \tag{2.3}$$

$$\sigma_{22} = 2\mu\frac{\lambda}{2\mu+\lambda}\gamma_{11} + 2\mu\frac{2(\mu+\lambda)}{2\mu+\lambda}\gamma_{22} \tag{2.4}$$

$$\mu_{13} = (\gamma+\varepsilon)\kappa_{13} \tag{2.5}$$

$$\mu_{23} = (\gamma+\varepsilon)\kappa_{23} \tag{2.6}$$

where λ and μ are the Lamé constants, α, γ, ε, are the Cosserat or micropolar moduli. We note that in the isotropic planar conditions there are only two classical, λ and μ and two independent Cosserat moduli, α and a combination $\gamma+\varepsilon$. Comparing systems of Eqs. (1.1)–(1.6) and (2.1)–(2.6) and expressing the Lamé constants through engineering moduli, we obtain the Young's modulus, E, shear modulus, G, and Poisson's ratio,v, in terms of the spring stiffnesses as follows:

$$E = \frac{2\sqrt{3}}{h}\frac{k_n+k_s}{3k_n+k_s}k_n \tag{3.1}$$

$$G = \frac{\sqrt{3}}{4h}(k_n+k_s) \tag{3.2}$$

$$v = \frac{k_n-k_s}{3k_n+k_s} \tag{3.3}$$

It is seen that the ratio of the shear to normal stiffnesses controls the (macroscopic) Poisson's ratio of the assembly and allows its values to vary from -1 to 1/3 as follows

$$k_s/k_n \to 0 \;\Rightarrow\; v \to 1/3 \tag{4.1}$$

$$k_s/k_n \to \infty \;\Rightarrow\; v \to -1 \tag{4.2}$$

It is interesting that in 3D, similar structures but with isotropic distribution of contacts exhibit the macroscopic Poisson's in the range between -1 and 1/4, Pasternak and Dyskin (2008a).

It can be observed that negative values of the Poisson's ratio can only be obtained when the shear to normal stiffness ratio is greater than one. Furthermore, to achieve large values of NPR, one needs a very high stiffness ratio of the bond between the discs. Another interesting observation is that the expression for the Poisson's ratio in Eq. (3.3) does not include the stiffness of the rotational spring and subsequently coincides with the one previously obtained by Bathurst and Rothenburg (1988). Thus the use of higher order theories does not produce new parameters in design of the auxetic microstructures (see also Pasternak and Dyskin, 2012).

Eqs. (3) can approximate the behavior of an assembly of deformable elastic bodies if one neglects the non-linearity produced by Hertzian contacts. Consequently, NPR in the assembly of deformable structural units is also controlled by the ratio of shear to normal contact stiffnesses. It is important to note that in this case, the stiffnesses merely depend on the structural characteristics of the basic unit. Hence, in order to build an isotropic auxetic material, we only need to design a hexagonally symmetric structural unit with the high shear to normal stiffness ratio.

In the next section, a novel type of auxetic isotropic structural units is developed based on these principles. NPR behavior of the proposed structure is studied numerically using both continuum approach and direct structural analysis of periodic assemblies.

3. Isotropic 2D auxetic assemblies

Based on the framework developed in Section 2, a unit with the high shear to normal stiffness ratio is proposed in this section. To achieve this goal, we replace the solid discs used in the continuum model with a flexible closed frame. Then, in order to enhance the shear stiffness of the frame, we introduce a reinforcing core into the unit. Following this concept, Fig. 1(a) sketches such a unit, which consists of a flexible frame made of circular arches and a solid regular hexagon used as a core. This unit has hexagonal symmetry required to achieve isotropy of the assembly. Note that the hexagon core can be replaced with other shapes or be partly solid as long as it is considerably stiffer than the frame and the hexagonal symmetry is preserved.

Next, we analyse these reinforced units in terms of the macroscopic Poisson's ratio they exhibit.

3.1. Arch-frame reinforced units

A reference unit with a rigid hexagonal core and a frame made of circular arches shown in Fig. 1(a) is considered. We assume a regular hexagonal arrangement of identical units, where each unit contacts six others at the apex of each arch spring. The core is assumed infinitely rigid, while the frame is linear elastic with a conventional Poisson's ratio. As a result, all deformations occurring in the unit are due to bending and stretching of the arches. Thus determining the contact stiffnesses of the unit is reduced to calculating the stiffnesses of the arch frame:

$$k_n = \left.\frac{P_V}{W_V}\right|_{P_H=0} \tag{5.1}$$

$$k_s = \left.\frac{P_H}{W_H}\right|_{P_V=0} \tag{5.2}$$

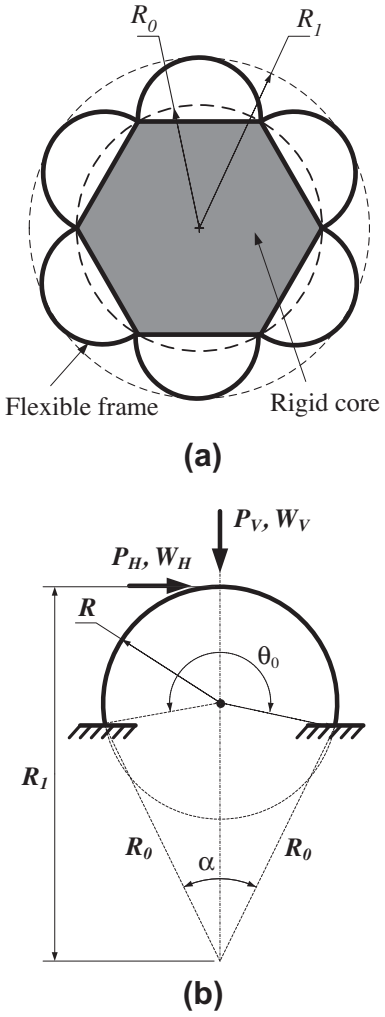

Fig. 1. A reinforced unit: (a) geometry of the unit; (b) the arch-spring.

where W_H and W_V are the tangential and normal displacements at the arch apex and P_H and P_V are the applied forces (see Fig. 1(b)). Note that the rotational contact stiffness is not considered here since it does not appear in the expression for the Poisson's ratio, Eq. (3.3), which is the main focus of this study. However, if required, the rotational stiffness can be calculated in a similar manner as a ratio between the applied moment and the bending rotation at the arch apex.

Three aspects of the analysis of the structural system at hand are considered: the unit geometry, the core-frame connection and bonding between the units in the assembly. The geometry of the unit is defined using the ratio, f, of its outer radius, R_1 and the circumscribed radius of the hexagonal core, R_0 (see Fig. 1):

$$f = R_1/R_0 \tag{6}$$

The arch radius R and the sectorial angle θ_0 of the arch, Fig. 1(b), can be expressed in terms of this ratio as:

$$R = \frac{f^2 - 2f\cos(\alpha/2) + 1}{2(f - \cos(\alpha/2))} R_0 \tag{7.1}$$

$$\theta_0 = 2\arcsin\left(\frac{2f\sin(\alpha/2) - \sin(\alpha)}{f^2 - 2f\cos(\alpha/2) + 1}\right) \tag{7.2}$$

where α is the angle of the arch span, Fig. 1(b). Angle α depends upon the shape of the core; for the hexagonal core it is equal to 60°. Varying the ratio f, various shapes of the unit can be achieved starting with very low curvature profile up to almost closed circular arches. This parameter is however bounded by (1) a restriction that the arch curvature is directed outwards the unit and (2) the necessity to avoid the intersection of adjacent arches. Combining these restrictions gives:

$$\cos(\alpha/2) < f < \frac{\cos(\alpha/2)}{1 - \sin(\alpha/2)} \tag{8}$$

Three structural types of the core-frame connections are shown in Fig. 2(a). We assume that the connection allows no displacements and the type of the connection is defined by its ability to prevent the

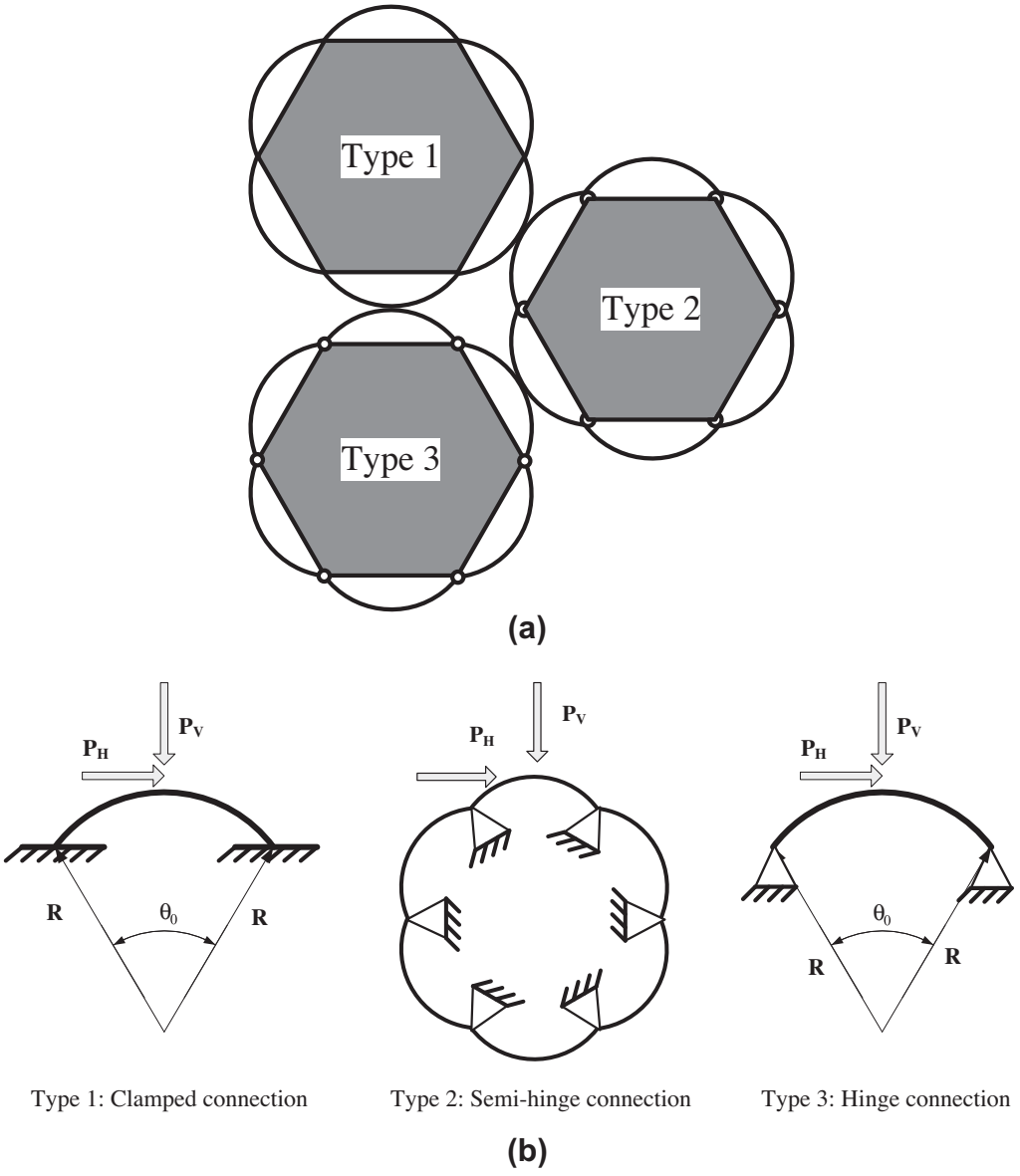

Fig. 2. Assembly of reinforced units: (a) three types of frame-core connection; (b) structural models for calculation of the arch-spring stiffnesses: loading and boundary conditions.

rotation between the frame and the core. The first type of connection is a fully clamped perfect bond between all parts of the unit. The connection of the second type permits free rotation between the core and the frame. However, the frame has no hinges (the arches are clamped to each other) and this link is called a semi-hinge. In contrast, the connection of the third type is fully hinged such that free rotations between all parts of the joint are allowed.

The computational models of the arch stiffnesses for each connection type are shown in Fig. 2(b). Since in cases 1 and 3 there is no interaction between the parts of the frame, the stiffnesses can be computed using a single arch coil of the frame. On the other hand, in case 2, the adjoining arches interact with each other through a bending moment transferred over the connection. As a result, the whole frame has to be solved in this case.

Last but not least, the structural aspect considered in this study is the connection between the units in the assembly. As the real contacts between the structural elements are not points, the effect of contact area has to be addressed as well. For the sake of simplicity, we assume that the contact forces are uniformly distributed over the contact area. Consequently, the concentrated loads are replaced with uniformly distributed ones in the arch stiffness computations. This description allows us to analyse the influence of the contact area on the mechanical behaviour of the assembly.

3.2. Structural analysis of arch frames

The direct stiffness method is employed for the structural analysis of the arch frames. In this method, the exact stiffness relations of structural members represented through the stiffness matrix are used for computing forces and displacements (Weaver and Gere, 1990). In order to obtain a solution for different arch thicknesses, the stiffness matrix for an arch element is derived including the effect of transverse shear deformations (see Appendix B). To model the three abovementioned types of connections, a range of plane

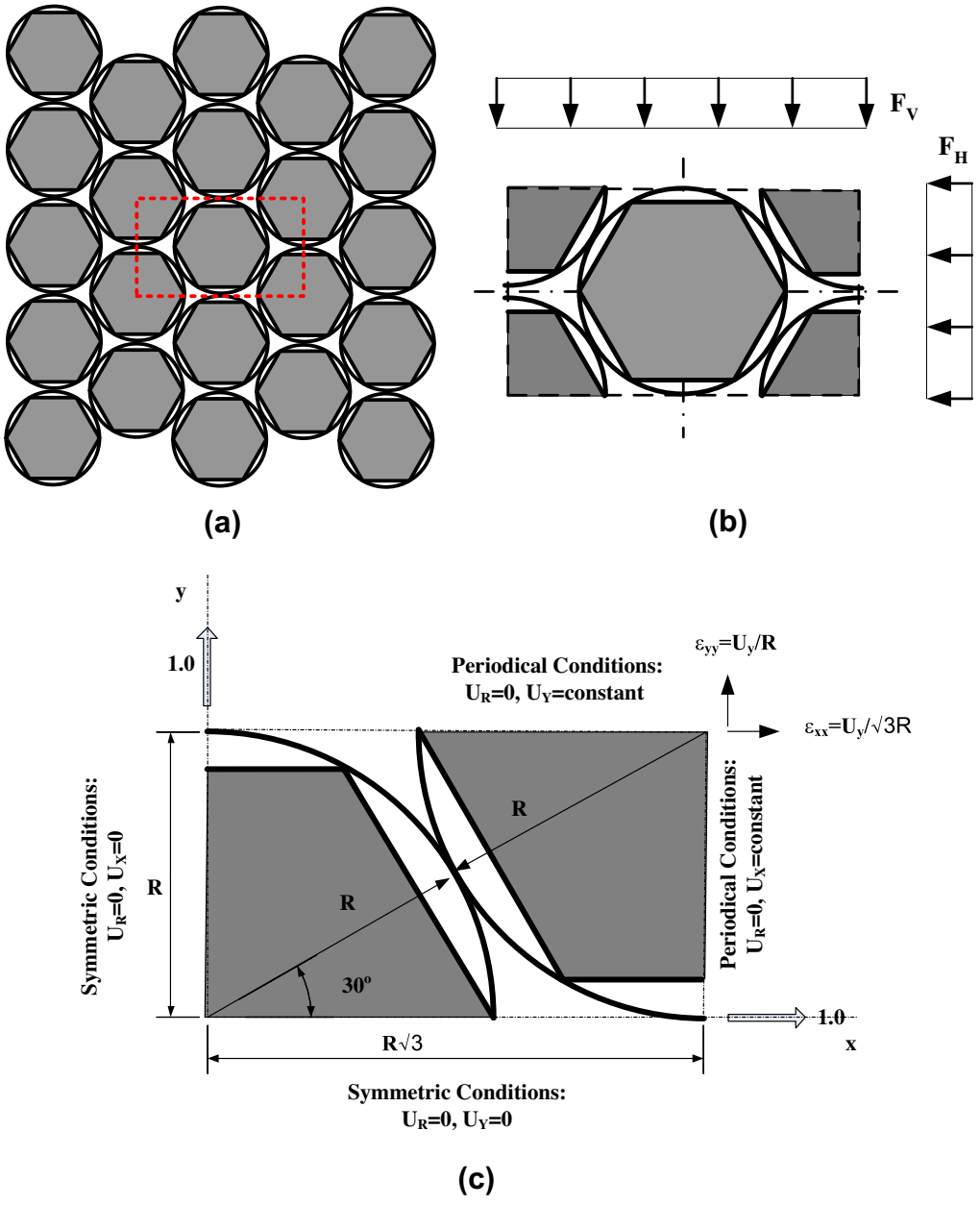

Fig. 3. Structural computational model of a periodic assembly of reinforced units with a ring shaped flexible frame: (a) Assembly with the periodicity cell indicated by a rectangle; (b) the representative (periodicity) cell; (c) the computational cell and the use of symmetry in both directions – loading and boundary conditions.

Table 1
Poisson's ratios for the ring-hexagon unit with various types of core-frame connection: the continuum approach vs. structural solution.

t/R	Connection type								
	Type 1 (clamped)			Type 2 (semi-hinge)			Type 3 (hinge)		
	Continuum model	Load in x dir	Load in y dir	Continuum model	Load in x dir	Load in y dir	Continuum model	Load in x dir	Load in y dir
0.005	−0.559	−0.559	−0.559	−0.466	−0.428	−0.428	−0.368	−0.368	−0.368
0.01	−0.568	−0.568	−0.568	−0.472	−0.442	−0.442	−0.373	−0.373	−0.373
0.015	−0.580	−0.580	−0.580	−0.482	−0.463	−0.463	−0.382	−0.382	−0.382
0.02	−0.593	−0.593	−0.593	−0.494	−0.487	−0.487	−0.393	−0.393	−0.393
0.025	−0.608	−0.607	−0.607	−0.508	−0.513	−0.513	−0.406	−0.406	−0.406
0.03	−0.620	−0.620	−0.620	−0.521	−0.537	−0.537	−0.420	−0.420	−0.420
0.035	−0.632	−0.632	−0.632	−0.535	−0.558	−0.558	−0.435	−0.435	−0.435
0.04	−0.641	−0.641	−0.641	−0.547	−0.577	−0.577	−0.449	−0.449	−0.449
0.045	−0.648	−0.648	−0.648	−0.558	−0.593	−0.593	−0.464	−0.463	−0.463
0.05	−0.654	−0.654	−0.654	−0.568	−0.605	−0.605	−0.477	−0.477	−0.477
0.055	−0.657	−0.657	−0.657	−0.576	−0.616	−0.616	−0.490	−0.489	−0.489
0.06	−0.660	−0.659	−0.659	−0.583	−0.623	−0.623	−0.501	−0.501	−0.501
0.065	−0.660	−0.660	−0.660	−0.589	−0.629	−0.629	−0.512	−0.511	−0.511
0.07	−0.660	−0.660	−0.660	−0.593	−0.633	−0.633	−0.521	−0.521	−0.521
0.075	−0.659	−0.658	−0.658	−0.597	−0.635	−0.635	−0.530	−0.529	−0.529
0.08	−0.657	−0.656	−0.656	−0.599	−0.636	−0.636	−0.537	−0.537	−0.537
0.085	−0.654	−0.653	−0.653	−0.601	−0.636	−0.636	−0.544	−0.544	−0.544
0.09	−0.650	−0.650	−0.650	−0.602	−0.635	−0.635	−0.550	−0.549	−0.549
0.095	−0.646	−0.646	−0.646	−0.602	−0.633	−0.633	−0.555	−0.555	−0.555
0.1	−0.641	−0.641	−0.641	−0.602	−0.630	−0.630	−0.559	−0.559	−0.559

frame elements is developed following the procedure presented in Weaver and Gere (1990) and Eisenberger (1991). This approach allows the analytical solution for all structural problems involved in this study.

3.3. Direct structural analysis of a periodic assembly of reinforced units

In order to verify the results obtained using the continuum homogenisation procedure, the direct structural analysis is performed. For demonstration purposes, the comparisons between the continuum and structural approaches are made for a single unit shape, *viz*. a ring reinforced by a hexagonal core. In this particular case all radii in Fig. 1(a) are the same and $f = 1$.

A regular isotropic arrangement of the assembled units is shown in Fig. 3(a). This assembly is periodic in both coordinate directions. Therefore, the analysis of this assembly can be performed using a representative cell (cell of periodicity, Fig. 3(a)), which is selected as shown in Fig. 3(b). The cell is loaded in two perpendicular directions, while the boundary conditions comply with the periodicity. In order to obtain a solution through the analytical stiffness method, a quarter part of the representative cell is considered. The geometry, loading, and boundary conditions of the corresponding computational model of the quarter cell are shown in Fig. 3(c). The symmetric boundary conditions imposed along edges $x = 0$ and $y = 0$ are

$$U_X|_{x=0} = U_R|_{x=0} = 0 \tag{9.1}$$

$$U_Y|_{y=0} = U_R|_{y=0} = 0 \tag{9.2}$$

where U_X and U_Y are the displacements in the x and y directions respectively, and U_R is the bending rotation in the plane of the assembly. The periodicity or continuity conditions are set along edges $x = \sqrt{3}R$ and $y = R$

$$U_R|_{x=\sqrt{3}R} = 0, U_X|_{x=\sqrt{3}R} = \textbf{constant} \tag{10.1}$$

$$U_R|_{y=R} = 0, U_Y|_{y=R} = \textbf{constant} \tag{10.2}$$

Due to the continuity constraint that the displacements are constant at the cell boundary, without any loss of generality, the distributed contact forces acting at the joints are replaced with the equivalent concentrated forces. The Poisson's ratio of the assembly is defined as usual:

$$\nu_{xy} = -\frac{\varepsilon_{yy}}{\varepsilon_{xx}} \tag{11.1}$$

$$\nu_{yx} = -\frac{\varepsilon_{xx}}{\varepsilon_{yy}} \tag{11.2}$$

where ε_{xx} and ε_{yy} are the normal strains in the x and y directions respectively, which are given as

$$\varepsilon_{xx} = \frac{U_X|_{x=\sqrt{3}R}}{\sqrt{3}R} \tag{12.1}$$

$$\varepsilon_{yy} = \frac{U_Y|_{y=R}}{R} \tag{12.2}$$

4. Microscopic structures associated with the same macroscopic continuum. Comparison with structural models

In this section we consider assemblies of reinforced units with the abovementioned three types of connection, which after homogenisation, produce the same macroscopic Poisson's ratio. We will develop structural models for each assembly and determine the macroscopic Poisson's ratio by determining the ratio of the corresponding strains. We will use these results to determine the accuracy of the continuum model and then analyse the role of different characteristics of the assemblies in the resulting Poisson's ratio.

We assume that all parts of the assembly have an equal unit width and are made of the same elastic material with the conventional Poisson's ratio of 0.3. The frame has a rectangular cross-section of thickness t. The calculated Poisson's ratio is presented as a function of the frame thickness normalised with respect to the circumscribed radius of the core.

4.1. Comparison with the continuum model

We first consider a regular assembly of the ring–hexagon units and analyse it using both continuum approach and direct structural analysis of a representative cell of the assembly (see Fig. 3). The analytical stiffness method is used to perform both the computations of the contact stiffnesses of the unit and the deformation analysis of the representative cell. All three possible types of the core-frame connections are considered. The units are assumed to be connected through point contacts (see Section 3.1). The analysis

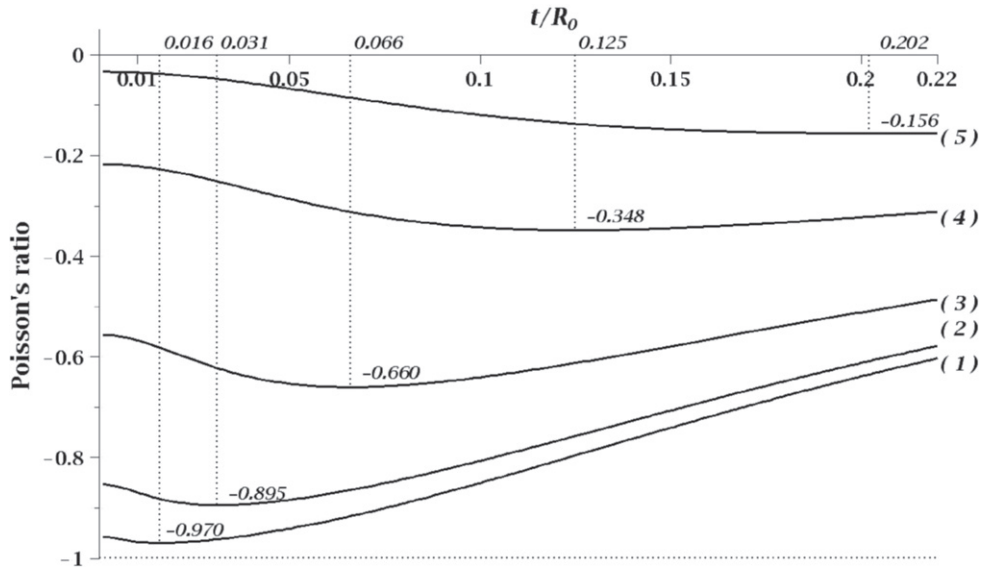

(a)

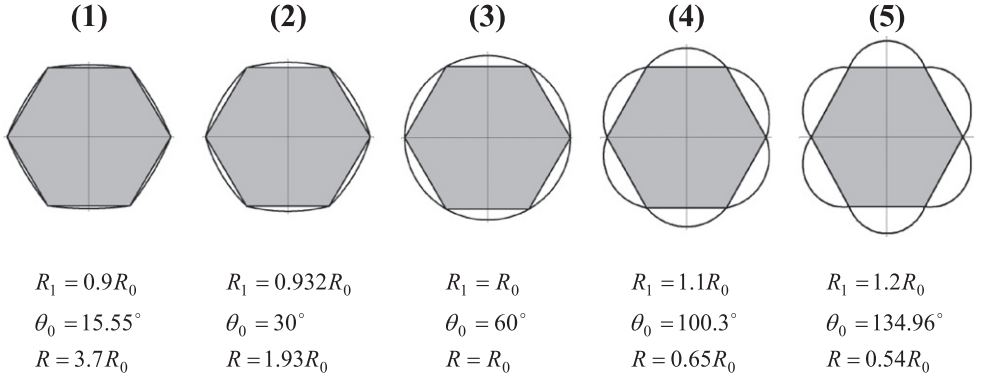

(b)

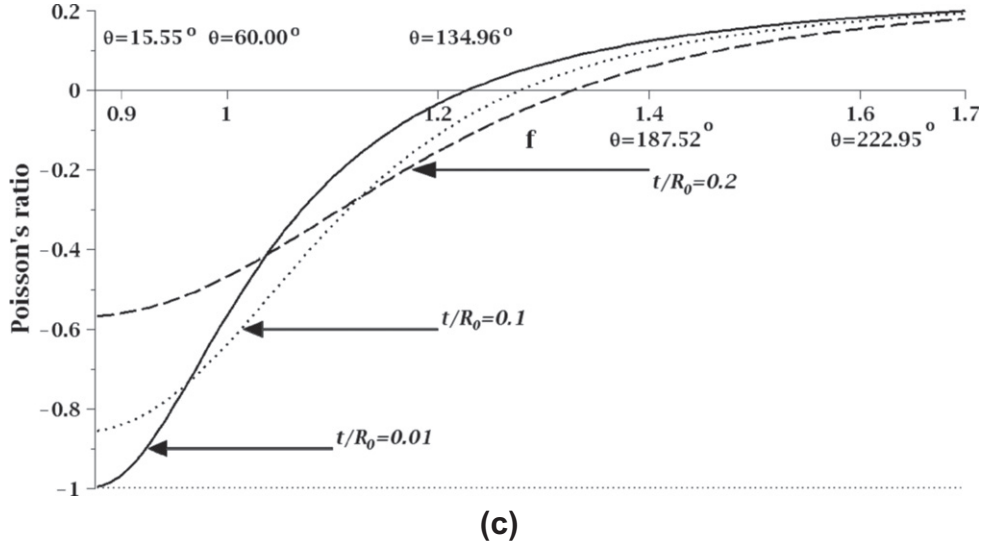

(c)

Fig. 4. Variation of the Poisson's ratio for different arch shapes; (a) the Poisson's ratio vs. aspect ratio of the arch-springs, f = 0.9, 0.932, 1, 1.1, 1.2; (b) the unit geometries, (c) the Poisson's ratio vs. the f ratio of unit geometry, t/R_0 = 0.01, 0.1, 0.2.

of the representative cell is carried out for two types of loading: in the x direction and in y direction (see Fig. 3).

Poisson's ratios computed using the continuum model and the structural model (for 2 directions of loading) are presented in

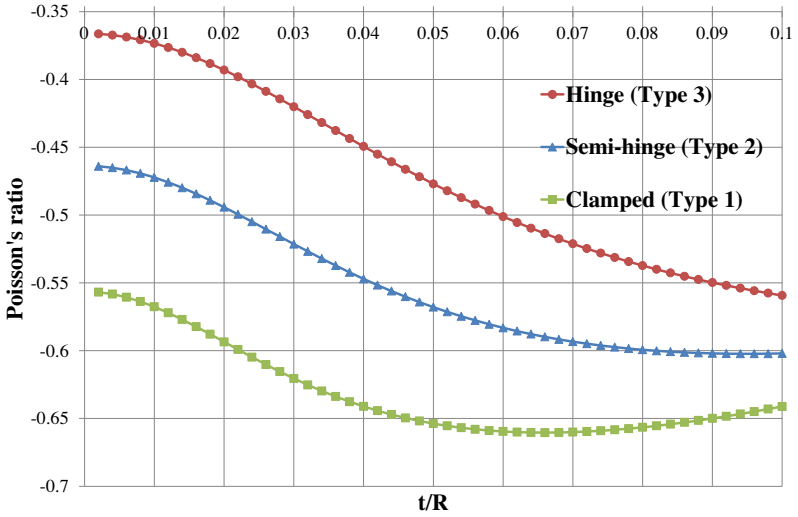

Fig. 5. Variation of the Poisson's ratio for the ring–hexagon unit for different types of core-frame connection.

Table 1 for three types of the core-frame connections. It is seen that for the connection types 1 and 3 the continuum approach and the structural analysis are in a complete agreement. However, in the case of semi-hinge connection (type 2), the continuum approach overestimates NPR for thin frames by up to 9% and underestimates it for thicker frames by up to 6.5%. The difference is ascribed to the fact that the model developed for an assembly of rigid particles is used for the assembly of elastic bodies. It has been discussed in Section 3.1 that each arch works independently in the case of the first and third types of the core-frame connections, while the second, semi-hinge type allows for the interaction between the arches. This interaction makes the deformations at the neighbouring contact points coupled. On the other hand, the homogenisation procedure developed in Section 2 only deals with rigid particles and does not account for the interaction between the contact points. Consequently, this continuum model provides very accurate results for the clamped and hinge types of the core-frame connections and gives a healthy approximation of Poisson's ratio for the semi-hinge type.

In the next section, this continuum approach is used to study structural characteristics of the reinforced units. In addition, the results obtained for different loading conditions reveal that the assembly exhibits isotropic behaviour for all three types of the core-frame connections in the whole range of the normalized thicknesses.

4.2. Arch-frame units: shape study

The different shapes of the arch-frame units are studied by varying the ratio f, Eq. (6). The core-frame connection is clamped and the concentrated loads are used for calculation of the stiffnesses. Fig. 4(a) presents the results for five different shapes of the arch frame unit displayed in Fig. 4(b). These figures reveal that this isotropic type of assembly exhibits auxetic behaviour along the whole range of the thicknesses. The largest NPR is observed in the case of the arches with smaller curvature (Case 1); for very thin arches it approaches the lower bound of -1. Negative values of the Poisson's ratio initially decrease with increase in the thickness of the arch frame, reaching the minimum of -0.97 at $t/R_0 = 0.016$ for Case 1. At the same time, the increase in the arch curvature reduces the values of the negative Poisson's ratio along the whole range of the thicknesses. The local minima (the maxima for NPR) shift from the region of very thin frames for the low curvature arches to thicker frames with higher curvatures. Plots of the Poisson's ratio vs. ratio f for fixed thickness ratios are shown in Fig. 4(c). It is seen that for low curvatures thinner frames are able to produce larger NPR values and this capability declines for higher curvatures. At the same time, the rate of this decline slows down when thicker frames are used. In addition, angles θ shown for each ratio f demonstrate that the half circle arch ($\theta = 180°$) is the maximum arch angle at which the proposed structure produces NPR.

While the low curvature shapes provide higher NPR, some units with higher curvature, such as the ring–hexagon units (Case 3 on Fig. 4(b); here $f = 1$, $R = R_0 = R_1$, $\theta = 60°$), are of interest due to their topological regularity. We investigate them in the following section.

4.3. Ring–hexagon units. Effect of core-frame connection

The effect of three types of core-frame connection (see Fig. 2) on the auxetic behaviour of an assembly of the ring-hexagon units is studied here. Fig. 5 shows the Poisson's ratio calculated using the continuum approach assuming point contacts between the units. The results reveal that the clamped connection yields the largest NPR up to -0.66 for $t/R = 0.066$. It is also seen that a change in the connection type from clamped to hinge decreases the values of the negative Poisson's ratio by 13–34%. Changing the connection type from the clamped to semi-hinge decreases NPR by up to 15%.

4.4. Ring–hexagon units: contact area study

In order to study the influence of the contact area between the units we compare the results obtained for point contacts (concentrated contact forces) with those obtained using the uniformly distributed contact forces. The length of the load distribution (the contact area), L_P is defined as

$$L_P = 2aR \tag{13}$$

where a is the dimensionless width of the contact area. Fig. 6 shows the variations of the Poisson's ratio for three types of the core-frame connection for various values of a. It is seen that an increase in the contact area reduces values of negative Poisson's ratio for all types of the core-frame connection. This effect is more pronounced in the case of the clamped core-frame connection providing up to 38% decrease in the NPR value when the contact area increases from a point, $a = 0$ to $a = 0.2$ and up to 33% for $a = 0.1$. At the same time, the more flexible types of the core-frame connection (types 2 and 3) are less sensitive to variations in the contact area. The difference

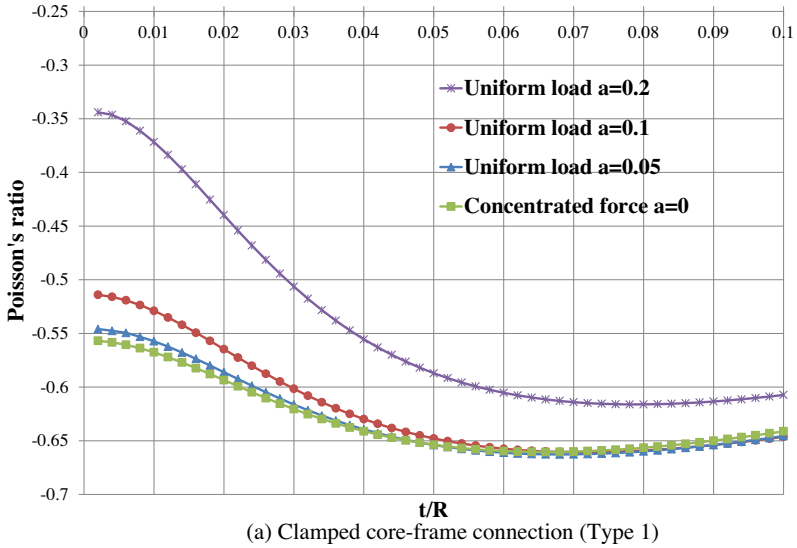

(a) Clamped core-frame connection (Type 1)

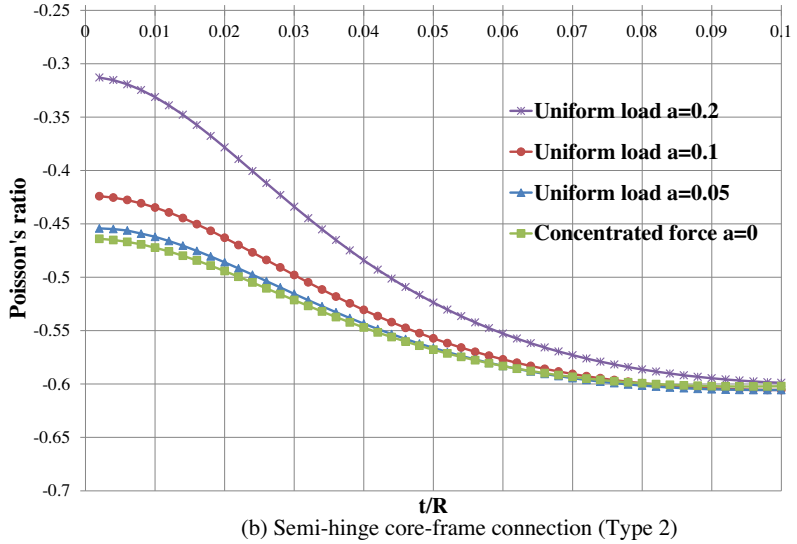

(b) Semi-hinge core-frame connection (Type 2)

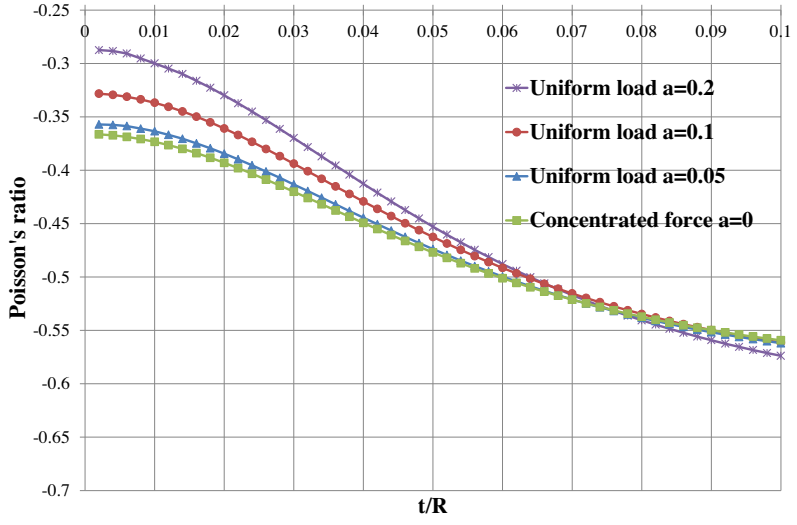

(c) Hinge core-frame connection (Type 3)

Fig. 6. Variation of the Poisson's ratio for the ring–hexagon units for different sizes of contact area between the units: (a) clamped core-frame connection (Type 1), (b) semi-hinge core-frame connection (Type 2), (c) hinge core-frame connection (Type 3).

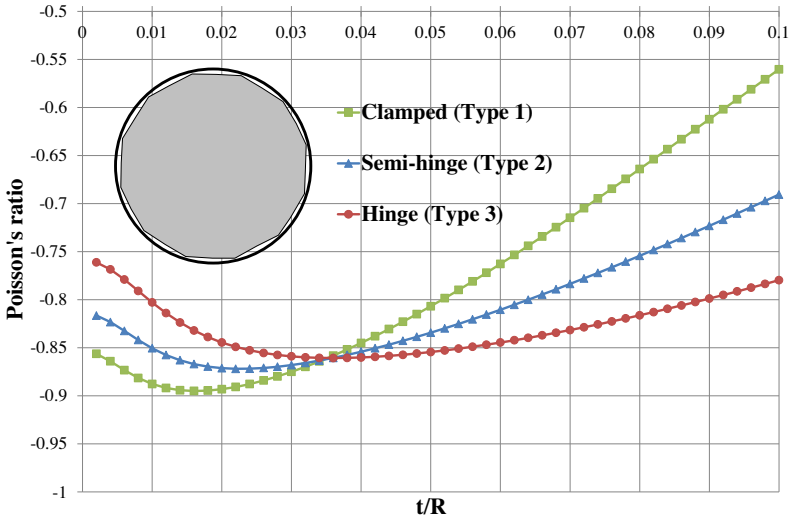

Fig. 7. The Poisson's ratio in the assemblies of ring–dodecagon units.

between the results obtained for $a = 0.05$ and $a = 0.2$ is up to 30% in the semi-hinge case (Type 2) and up to 20% in the hinge case (Type 3). The influence of the contact area becomes less noticeable as well for the thicker frames, such that for the connection Types 2 and 3 the results essentially coincide for all widths of the contact area.

4.5. Units of other types

In this section other types of reinforced units are introduced. First a basic unit consisting of a flexible ring and a rigid core of dodecagonal shape, Fig. 7, is considered. Fig. 7 presents the Poisson's ratio calculated for three types of the core-frame connections using the continuum model. It is seen that very high values of NPR are obtained in all cases. The largest NPR of -0.895 is observed in the clamped case at $t/R = 0.015$.

As another example, we consider a unit consisting of a hexagonal core with a different kind of a flexible frame – a polygonal frame consisting of straight bars. Four such frames are shown in Fig. 8(a). These units have geometry similar to the ring–hexagon units, Fig. 3. These frames also have rectangular cross-sections with thickness t. Fig. 8(a) shows the computational schemes for the corresponding spring frames. To study behaviour of these units, the contact stiffnesses are calculated using the classical beam theory. Introduction of these stiffnesses into the continuum formula (3.3) yields, after some algebra, explicit expressions for the Poisson's ratio for each type of the units (Fig. 8(a)):

Case 1:

$$\nu = \frac{\cos(\theta) + (t/R)^2(3/4 - 2\cos(\theta) + 5/4\cos^2(\theta))}{\cos(\theta) + 2 + (t/R)^2(13/4 - 8\cos(\theta) + 11/4\cos^2(\theta))} \tag{14.1}$$

Case 2:

$$\nu = \frac{\cos(\theta) + (t/R)^2(\cos^2(\theta) - \cos(\theta))/2}{\cos(\theta) + 2 + (t/R)^2(1 - 3/2\cos(\theta) + 1/2\cos^2(\theta))} \tag{14.2}$$

Case 3:

$$\nu = \frac{\cos(\theta) + (t/R)^2(1/4 - 3/2\cos(\theta) - 1/4\cos^2(\theta))}{\cos(\theta) + 2 + 3/4(t/R)^2(1 - \cos(\theta))^2} \tag{14.3}$$

Case 4:

$$\nu = \frac{\cos(\theta)}{\cos(\theta) + 2} \tag{14.4}$$

It is seen that the Poisson's ratio in Case 4 (Pinned, Hinge), Fig. 8(a) does not depend on the frame thickness, since in this case the frame merely deforms by stretching due to its pinned ends. In addition, it can be observed that when the ratio t/R tends to zero, the first three cases, Eqs. (14.1)–(14.3), coincide with Eq. (14.4). These expressions are plotted in Fig. 8(b) as a function of the sectorial angle, θ. The graphs demonstrate that this unit provides NPR for all types of connection when the opening angle θ is greater than 90°. The negative values of Poisson's ratio increase when this angle tends to 180° approaching the lower bound of -1.

Fig. 8(c) shows the Poisson's ratio as a function of the normalized thickness of the frame for $\theta = 150°$. (The angle $\theta = 150°$ is chosen, because for this angle the plane frame unit geometrically matches the ring–hexagon unit.) It is seen that the results for Cases 2 and 3 coincide in the whole range of the thicknesses. In addition, deviations of all values from the pinned-hinge case, the one which provides the largest NPR of -0.764, are not large (less than 13% difference).

5. Conclusions

Novel planar structures exhibiting isotropic auxetic behaviour on macroscopic level have been developed. A distinctive feature of these structures is the presence of a reinforcing core in each unit. The main role of the core is to increase the frame resistance to the tangential movement thus ensuring high shear stiffness, whereas the normal stiffness is low being controlled by the local bending response of the frame.

The structures we considered have hexagonal (six-fold) symmetry, which produces elastic isotropic properties in the plane perpendicular to the axis of the hexagonal symmetry. A macroscopic Cosserat continuum description for a planar assembly of rigid particles was obtained using the homogenisation procedure based on differential expansions. Based on this model a new design of auxetic materials was proposed- assemblies of units each consisting of a flexible frame reinforced by a rigid core. Different reinforced units with various frame and core shapes, internal structures,

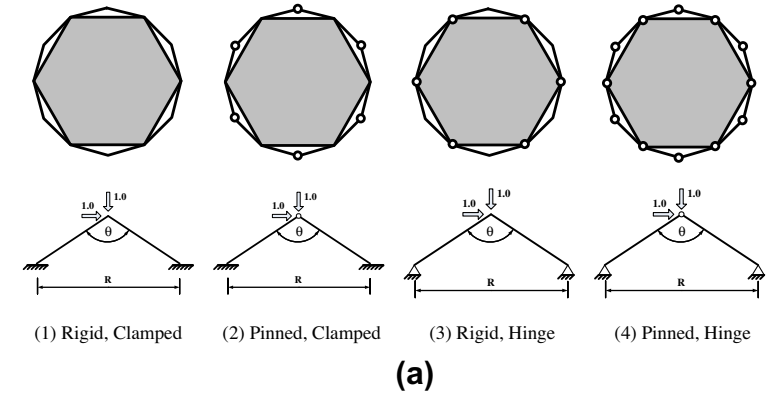

(a)

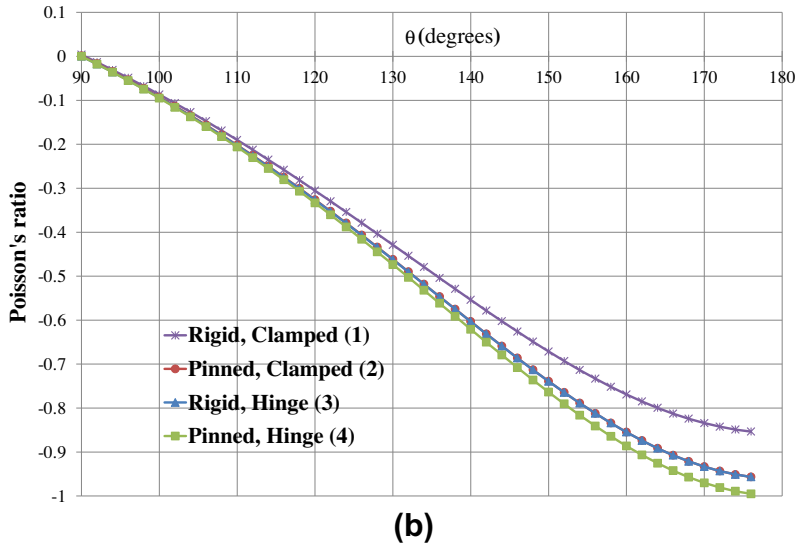

(b)

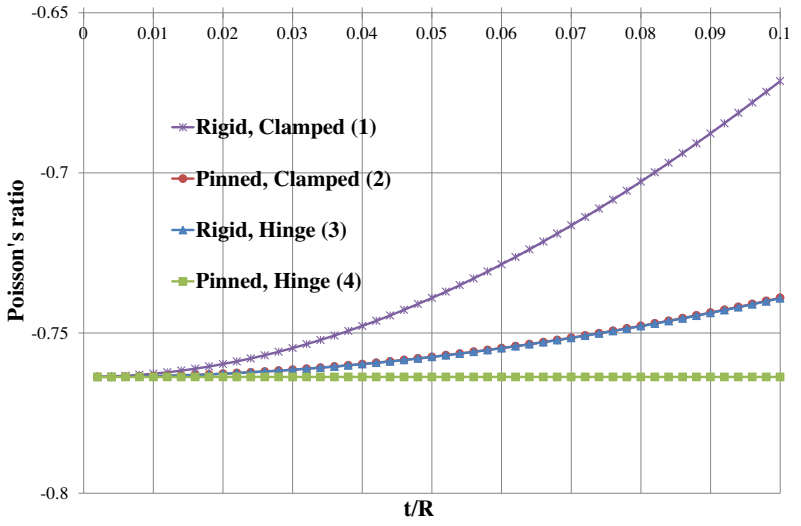

(c)

Fig. 8. The Poisson's ratio in assemblies of polygonal frame units: (a) hexagon core units with various core-frame connections and apex hinges, (b) the Poisson's ratio vs. the sectorial angle of the frame, $t/R = 0.1$, (c) the Poisson's ratio vs. the thickness-span ratio of the frame, $\theta = 150°$.

and bond dimensions were studied numerically. It was shown that these systems are able to provide the Poisson's ratio as low as −0.9.

The continuum homogenisation model originally developed for granulate materials composed of rigid grains was verified against the direct structural simulations of a periodical assembly of elastic structures. It was found that the accuracy of the continuum model depends upon the mechanical interactions between the contact points. The continuum approach yields very accurate results when the neighbouring arches of the frame deform independently. This happens when the arches have clamp and hinge connections. In the case of the semi-hinge connection (Type 2) the deformation of one arch affects the movement of the other. This coupling results

in the force–displacement relationship in one arch being dependent upon the deformation of the other. Since the continuum model presumes these deformations being independent one cannot expect the continuum model to identically reproduce the macroscopic behaviour of the structures with the semi-hinge connections. Indeed, the comparison between the results of the continuum model and the exact structural analysis shows that the results differ, but not much. Thus the continuum model gives a healthy balance between the simplicity and accuracy and can be used as a simple tool for design of auxetics.

Two types of frames were considered: the frame consisting of the arches supported by the vertices of the hexagonal core and the frame in the shape of polygons with hinges between the sides. The values of the negative Poisson's ratio in the case of the arches depend upon the frame geometry. In particular, the thinner the frame arches and the smaller the arch curvature, the higher the value of NPR. However the thickness cannot be decreased indefinitely; there is an optimum thickness where NPR reaches a maximum. The hinged polygonal frame on the other hand produces the NPRs independent of the thickness, but the values of the achievable NPRs are higher than those produced in structures with the arch frame.

We now have a new design principle– the introduction of the reinforcing core to the units and a suite of computational tools, both structural and simple continuum to analyse the behaviour of these structures. This approach can be extended to developing assemblies with different types of symmetry, non-uniform particle orientations and 3D assemblies.

Acknowledgements

The authors acknowledge the financial support from the Australian Research Council through the Discovery Grant DP0773839.

Appendix A. Homogenisation of 2D hexagonal structure by differential expansions. Derivation of 2D Cosserat continuum

A regular planar assembly of identical discs elastically bonded together is considered (see Fig. A1(a)). The assembly has regular hexagonal geometry where each disc contacts six others. We assume the plane stress conditions. Following Pasternak and Mühlhaus (2005), the interaction between two neighboring discs is described using normal and tangential (shear) translational springs of stiffness k_n and k_s respectively, and rotational springs of stiffness k_ϕ. Each disc has three independent degrees of freedom: two translations u_1 and u_2 and rotation ϕ_3. Discs themselves are considered to be absolutely rigid, so there is no out-of-plane component of displacement u_3. At the same time, the other independent rotations, ϕ_1 and ϕ_2, are assumed zero to keep the assembly planar.

We consider the cell of periodicity, Fig. A1(b) as a representative volume element. The volume of the cell is:

$$V_c = 2\sqrt{3}r^2 h \tag{A.1}$$

where r is the radius of the discs and h is the thickness of the assembly. The orientation of the contact between a pair of discs is described using the alignment angle α, which identifies the relative position of two discs. A local coordinate system is introduced by rotating the global system by an angle α (see Fig. A1(c)).

The coordinate transformation from the global to local coordinate systems is given as

$$\begin{Bmatrix} \bar{u}_1 \\ \bar{u}_2 \\ \bar{\phi}_3 \end{Bmatrix} = \begin{bmatrix} \cos(\alpha) & \sin(\alpha) & 0 \\ -\sin(\alpha) & \cos(\alpha) & 0 \\ 0 & 0 & 1 \end{bmatrix} \begin{Bmatrix} u_1 \\ u_2 \\ \phi_3 \end{Bmatrix} \tag{A.2}$$

where the barred notation designates the vector components in the local coordinate system. The potential discrete energy of the two-disc interaction reads

$$W_\alpha = \frac{1}{2}k_n(\bar{u}_{\alpha 1} - \bar{u}_1)^2 + \frac{1}{2}k_s\left((\bar{u}_{\alpha 2} - r\bar{\phi}_{\alpha 3}) - (\bar{u}_2 + r\bar{\phi}_3)\right)^2 + \frac{1}{2}k_\phi(\bar{\phi}_{\alpha 3} - \bar{\phi}_3)^2 \tag{A.3}$$

where $\bar{u}_1, \bar{u}_2, \bar{\phi}_3$ and $\bar{u}_{\alpha 1}, \bar{u}_{\alpha 2}, \bar{\phi}_{\alpha 3}$ are the displacements and rotations of disc at the origin and a neighbouring disc at the angle α. Applying the coordinate transformation (A.2) to Eq. (A.3) we obtain the discrete energy in terms of the global displacements and rotations as follows:

$$W_\alpha = \frac{1}{2}k_n(\cos(\alpha)(u_{\alpha 1} - u_1) + \sin(\alpha)(u_{\alpha 2} - u_2))^2 + \frac{1}{2}k_s(-\sin(\alpha)(u_{\alpha 1} - u_1) + \cos(\alpha)(u_{\alpha 2} - u_2) - r(\phi_{\alpha 3} + \phi_3))^2 + \frac{1}{2}k_\phi(\phi_{\alpha 3} - \phi_3)^2 \tag{A.4}$$

In order to obtain a continuum description, we homogenise the discrete energy. The discrete displacements and rotations are replaced with the continuous ones and then they are expanded into Taylor series keeping the linear terms. In the global coordinates this expansion for an arbitrary continuously differentiable function $f(x_1,x_2)$ reads

$$f_\alpha = f(x_1, x_2) + 2r\cos(\alpha)\frac{\partial f(x,y)}{\partial x} + 2r\sin(\alpha)\frac{\partial f(x,y)}{\partial y} \tag{A.5}$$

The homogenised spring energy of the two-disc interaction is obtained as a function of angle α as follows:

$$W_\alpha = 2r^2k_n\left(\cos^2(\alpha)\gamma_{11} + \cos(\alpha)\sin(\alpha)(\gamma_{12} + \gamma_{21}) + \sin^2(\alpha)\gamma_{22}\right)^2 + 2r^2k_s\left(-\sin^2(\alpha)\gamma_{12} - \cos(\alpha)\sin(\alpha)(\gamma_{11} - \gamma_{22}) + \cos^2(\alpha)\gamma_{21}\right)^2 + 2r^2k_\phi(\cos(\alpha)\kappa_{13} + \sin(\alpha)\kappa_{23})^2 \tag{A.6}$$

where the Cosserat continuum deformation measures, strains γ_{ij} and curvatures κ_{ij}, are defined following Nowacki (1970) as

$$\begin{aligned} \gamma_{11} &= u_{1,1} \\ \gamma_{12} &= u_{2,1} - \phi_3 \\ \gamma_{21} &= u_{1,2} + \phi_3 \\ \gamma_{22} &= u_{2,2} \\ \kappa_{13} &= \phi_{3,1} \\ \kappa_{23} &= \phi_{3,2} \end{aligned} \tag{A.7}$$

The total energy density of the cell is obtained by a summation of the spring energy of three contacts at $\alpha = 0°$, 60°, and 120° (see Fig. A1(b)) over the cell volume.

$$W = \frac{\sqrt{3}}{8h}\left((k_n + 3k_s)\gamma_{21}^2 + 2(k_n - k_s)\gamma_{12}\gamma_{21} + (k_n + 3k_s)\gamma_{12}^2 + (3k_n + k_s)\gamma_{11}^2 + (3k_n + k_s)\gamma_{22}^2 + 2(k_n - k_s)\gamma_{11}\gamma_{22} + 4k_\phi\kappa_{13}^2 + 4k_\phi\kappa_{23}^2\right) \tag{A.8}$$

Variation of the total energy density, Eq. (A.8), with respect to the deformation measures (A.7), yields the following constitutive equations of the equivalent Cosserat continuum

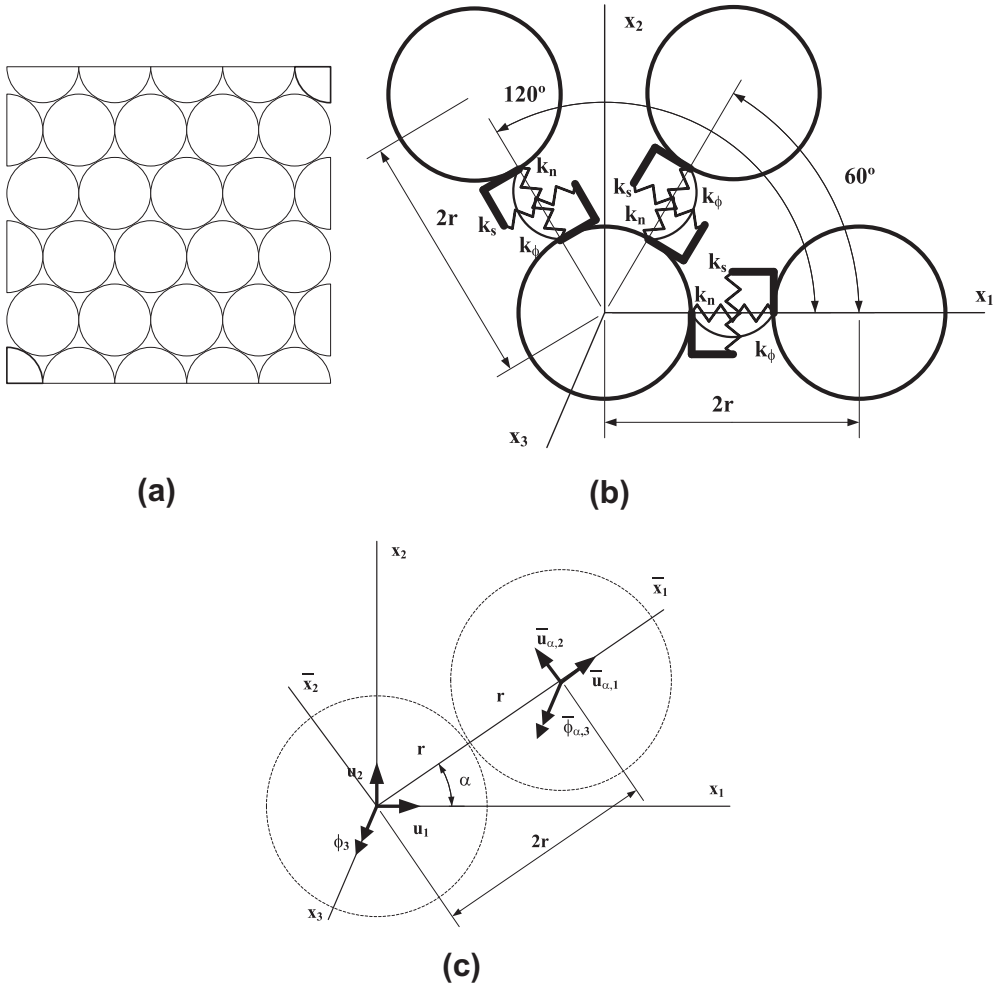

Fig. A1. A planar hexagonal assembly (a), the representative cell (b) and two contacting discs (c).

$$
\begin{aligned}
\sigma_{11} &= \frac{\sqrt{3}}{4h}((3k_n + k_s)\gamma_{11} + (k_n - k_s)\gamma_{22}) \\
\sigma_{12} &= \frac{\sqrt{3}}{4h}((k_n + 3k_s)\gamma_{12} + (k_n - k_s)\gamma_{21}) \\
\sigma_{21} &= \frac{\sqrt{3}}{4h}((k_n - k_s)\gamma_{12} + (k_n + 3k_s)\gamma_{21}) \\
\sigma_{22} &= \frac{\sqrt{3}}{4h}((k_n - k_s)\gamma_{11} + (3k_n + k_s)\gamma_{22}) \\
\mu_{13} &= \frac{\sqrt{3}}{h}k_\phi\kappa_{13} \\
\mu_{23} &= \frac{\sqrt{3}}{h}k_\phi\kappa_{23}
\end{aligned}
\tag{A.9}
$$

On the other hand, the constitutive relations of isotropic Cosserat media are defined as (Nowacki, 1970)

$$
\begin{aligned}
\sigma_{ij} &= ((\mu - \alpha)\delta_{jk}\delta_{il} + (\mu + \alpha)\delta_{jl}\delta_{ik} + \lambda\delta_{ij}\delta_{kl})\gamma_{kl} \\
\mu_{ij} &= ((\gamma - \varepsilon)\delta_{jk}\delta_{il} + (\gamma + \varepsilon)\delta_{jl}\delta_{ik} + \beta\delta_{ij}\delta_{kl})\kappa_l
\end{aligned}
\tag{A.10}
$$

where λ and μ are the Lamé constants, while α, γ, ε, and β are the Cosserat or micropolar parameters and summation of repeated indexes is presumed. Applying the plane stress assumption, the 3D relations of Eq. (A.10) are reduced to

$$
\begin{aligned}
\sigma_{11} &= 2\mu\frac{2(\mu+\lambda)}{2\mu+\lambda}\gamma_{11} + 2\mu\frac{\lambda}{2\mu+\lambda}\gamma_{22} \\
\sigma_{12} &= (\mu - \alpha)\gamma_{21} + (\mu + \alpha)\gamma_{12} \\
\sigma_{21} &= (\mu + \alpha)\gamma_{21} + (\mu - \alpha)\gamma_{12} \\
\sigma_{22} &= 2\mu\frac{\lambda}{2\mu+\lambda}\gamma_{11} + 2\mu\frac{2(\mu+\lambda)}{2\mu+\lambda}\gamma_{22} \\
\mu_{13} &= (\gamma + \varepsilon)\kappa_{13} \\
\mu_{23} &= (\gamma + \varepsilon)\kappa_{23}
\end{aligned}
\tag{A.11}
$$

Introducing of the engineering moduli in Lamé constants we obtain

$$
\begin{aligned}
\sigma_{11} &= \frac{E}{1-\nu^2}\gamma_{11} + \frac{E\nu}{1-\nu^2}\gamma_{22} \\
\sigma_{12} &= (\mu - \alpha)\gamma_{21} + (\mu + \alpha)\gamma_{12} \\
\sigma_{21} &= (\mu + \alpha)\gamma_{21} + (\mu - \alpha)\gamma_{12} \\
\sigma_{22} &= \frac{E\nu}{1-\nu^2}\gamma_{11} + \frac{E}{1-\nu^2}\gamma_{22} \\
\mu_{13} &= (\gamma + \varepsilon)\kappa_{13} \\
\mu_{23} &= (\gamma + \varepsilon)\kappa_{23}
\end{aligned}
\tag{A.12}
$$

Comparing the systems of Eqs. (A.9) and (A.12), we obtain the explicit expressions for the constitutive parameters of the equivalent Cosserat continuum as a function of the spring stiffness. The classical material properties, the Young's modulus E, the Poisson's ratio ν, and the shear modulus G are

$$E = \frac{2\sqrt{3}}{h}\frac{k_n + k_s}{3k_n + k_s}k_n$$
$$\nu = \frac{k_n - k_s}{3k_n + k_s} \tag{A.13}$$
$$G = \frac{\sqrt{3}}{4h}(k_n + k_s)$$

At the same time, there are only two non-zero Cosserat constants in this 2D formulation:

$$\gamma + \varepsilon = \frac{\sqrt{3}}{h}k_\phi$$
$$\alpha = \frac{\sqrt{3}}{2h}k_s \tag{A.14}$$

Appendix B. Derivation of the stiffness matrix for arch elements

The elements of the stiffness matrix are defined as holding actions at the end of an unloaded arch member due to unit displacements and rotations in the directions of 6 degrees of freedom shown in Fig. B1(a). In order to include shear deformations, the stiffness matrix is derived as an inverse of the corresponding flexibility matrix (Eisenberger, 1991). The flexibility matrix is obtained using the unit load method (Weaver and Gere, 1990), where the flexibility coefficients are defined as displacements due to the unit loads. To develop the flexibility matrix, an element shown in Fig. B1(b) is considered. The strain energy of an arch of radius R and opening angle θ_0 reads

$$U = \int_0^{\theta_0}\left(\frac{M^2}{2EI} + \frac{N^2}{2EA} + \frac{kQ^2}{2GA}\right)R\,d\theta \tag{B.1}$$

where M, N, and Q are the bending moment, the axial and shear forces respectively, G and E are the shear and Young's moduli, I and A are the moment of inertia and the area of the arch's cross-section, k is the shear correction factor. The shear correction factor is included to compensate for the discrepancy between the assumed constant distribution of shear stresses and the true parabolic state (Timoshenko and Goodier, 1982). The internal forces are defined as a function of angle θ (see Fig. B1(b)):

$$N(\theta) = -X_1\cos(\theta) + X_2\sin(\theta) \tag{B2.1}$$
$$Q(\theta) = X_1\sin(\theta) - X_2\cos(\theta) \tag{B2.2}$$
$$M(\theta) = X_1R(1 - \cos(\theta)) + X_2R\sin(\theta) - X_3 \tag{B2.3}$$

Adopting Castigliano's second theorem (Timoshenko and Goodier, 1982), the flexibility coefficients at the left end of the arch are obtained through differentiation of the strain energy with respect to the unit loads:

$$f_{ij} = \left.\frac{\partial U}{\partial X_i}\right|_{X_{j=i}=1, X_{j\neq i}=0}, \quad i = 1\ldots3, \quad j = 1\ldots3 \tag{B3.3}$$

Inverting the 3×3 matrix f_{ij}, the stiffnesses corresponding to the unit displacements in the directions one and two, and the rotation in the third coordinate direction are computed. The remaining terms of the stiffness matrix are found based on the equilibrium conditions of the element and symmetry of the matrix.

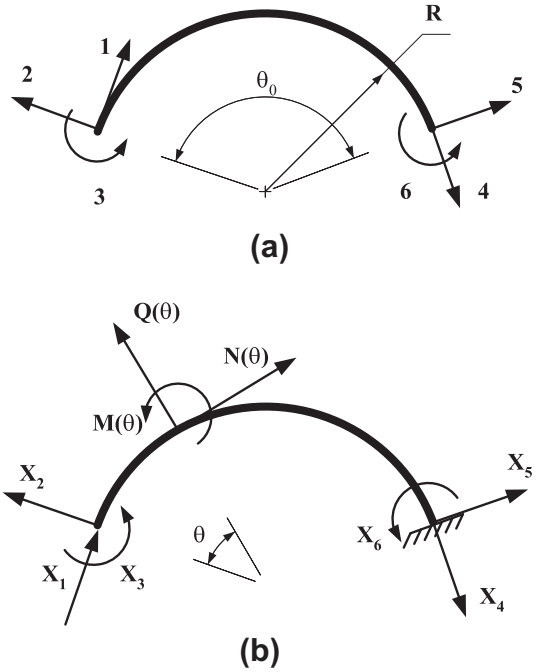

Fig. B1. Arch element with 6 degrees of freedom (DOF): (a) geometry and DOF definition, (b) holding actions and internal forces.

References

Alderson, A., Alderson, K.L., 2007. Auxetic materials. Proceedings of the Institution of Mechanical Engineers Part G: Journal of Aerospace Engineering 221 (4), 565–575.

Alderson, K.L., Evans, K.E., 1992. The fabrication of microporous polyethylene having a negative Poisson's ratio. Polymer 33 (20), 4435–4438.

Alderson, K.L., Evans, K.E., 1997. Modelling concurrent deformation mechanism in auxetic microporous polymers. Journal of Materials Science 32, 2797–2809.

Alderson, A., Evans, K.E., 2001. Rotation and dilation deformation mechanism for auxetic behaviour in the α-cristolobite tetrahedral framework structure. Physics and Chemistry of Minerals 28 (10), 711–718.

Alderson, K.L., Simkins, V.R., Coenen, V.L., Davies, P.J., Alderson, A., Evans, K.E., 2005. How to make auxetic fibre reinforced composites. Physica Status Solidi B 242 (3), 509–518.

Attard, D., Grima, J.N., 2011. Modelling of hexagonal honeycombs exhibiting zero Poisson's ratio. Physica Status Solidi B 248 (1), 52–59.

Attard, D., Manicaro, E., Grima, J.N., 2009a. On rotating rigid parallelograms and their potential for exhibiting auxetic behaviour. Physica Status Solidi B 246 (9), 2033–2044.

Attard, D., Manicaro, E., Gatt, R., Grima, J.N., 2009b. On the properties of auxetic rotating stretching squares. Physica Status Solidi B 246 (9), 2045–2054.

Bathurst, R.J., Rothenburg, L., 1988. Note on a random isotropic granular material with negative Poisson's ratio. International Journal of Engineering Science 26 (4), 373–383.

Bianchi, M., Scarpa, F., Banse, M., Smith, C.W., 2011. Novel generation of auxetic open cell foams for curved and arbitrary shapes. Acta Materialia 59, 686–691.

Blumenfeld, R., 2005. Auxetic strains- insight from iso-auxetic materials. Molecular Simulation 31 (13), 867–871.

Caddock, B.D., Evans, K.E., 1989. Microporous materials with negative Poisson's ratios: 1. Microstructure and mechanical properties. Journal of Physics D: Applied Physics 22 (12), 1877–1882.

Chan, N., Evans, K.E., 1997. Fabrication methods for auxetic foams. Journal of Material Science 32, 5945–5953.

Choi, J.B., Lakes, R.S., 1992a. Nonlinear properties of metallic cellular materials with a negative Poisson's ratio. Journal of Materials Science 27 (19), 5375–5381.

Choi, J.B., Lakes, R.S., 1992b. Nonlinear properties of polymer cellular materials with a negative Poisson's ratio. Journal of Materials Science 27 (19), 4678–4684.

Choi, J.B., Lakes, R.S., 1996. Fracture toughness of re-entrant foam materials with a negative Poisson's ratio: experiment and analysis. International Journal of Fracture 80, 73–83.

Coenen, V.L., Alderson, K.L., 2011. Mechanisms of failure in the static indentation resistance of auxetic carbon fibre laminates. Physica Status Solidi B 248 (1), 66–72.

Donoghue, J.P., Alderson, K.L., Evans, K.E., 2009. The fracture toughness of composite laminates with a negative Poisson's ratio. Physica Status Solidi B 246, 2011–2017.

Eisenberger, M., 1991. Stiffness matrices for non-prismatic members including transverse shear. Computer and Structures 40 (4), 831–835.

Evans, K.E., Alderson, A., 2000. Auxetic materials: functional materials and structures from lateral thinking! Advanced Materials 12 (9), 617–628.

Evans, K.E., Caddock, B.D., 1989. Microporous materials with negative Poisson's ratios: II. Mechanisms and interpretation. Journal of Physics D: Applied Physics 22 (12), 1883–1887.

Evans, K.E., Nkansah, M.A., Hutchinson, I.J., Rogers, S.C., 1991. Molecular network design. Nature. 353 (6340), 124.

Gaspar, N., 2010. A granular material with a negative Poisson's ratio. Mechanics of Materials 42, 673–677.

Gaspar, N., Ren, X.J., Smith, C.W., Grima, J.N., Evans, K.E., 2005. Novel honeycombs with auxetic behaviour. Acta Materialia 53, 2439–2445.
Gaspar, N., Smith, C.W., Alderson, A., Grima, J.N., Evans, K.E., 2011. A generalised three-dimensional tethered-nodule model for auxetic materials. Journal of Materials Science 46, 372–384.
Grima, J.N., Alderson, A., Evans, K.E., 2005. Auxetic behaviour from rotating rigid units. Physica Status Solidi B 242 (3), 561–575.
Grima, J.N., Gatt, R., Ravirala, N., Alderson, A., Evans, K.E., 2006. Negative Poisson's ratios in cellular foam materials. Materials Science and Engineering A 423, 214–218.
Grima, J.N., Cassar, R.N., Gatt, R., 2009. On the effect of hydrostatic pressure on the auxetic character of NAT-type silicates. Journal of Non-Crystalline Solids 355, 1307–1312.
Grima, J.N., Manicaro, E., Attard, D., 2010. Auxetic behaviour from connected different-sized squares and rectangles. Proceedings of the Royal Society A 467, 439–458.
Hall, L.J., Coluci, V.R., Douglas, S.G., Kozlov, M.E., Zhang, M., Dantas, S.O., Baughman, R.H., 2008. Sign change of Poisson's ratio for carbon nanotube sheets. Science 320, 504–507.
Jayanty, S., Crowe, J., Berhan, L., 2011. Auxetic fibre networks and their composites. Physica Status Solidi B 248 (1), 73–81.
Kolpakov, A.G., 1985. Determination of the average characteristics of elastic frameworks. Applied Mathematics and Mechanics 49, 739–745.
Kowalik, M., Wojciechowski, K.W., 2008. The free energy of hard dimer solids revisited. Journal of Non-Crystalline Solids 354, 4354–4358.
Lakes, R., 1987. Foam structures with a negative Poisson's ratio. Science 235, 1038–1040.
Landau, L.D., Lifshitz, E.M., 1986. Theory of Elasticity. Pergamon Press, Oxford.
Lim, T.-C., 2009. Out-of-plane modulus of semi-auxetic laminates. European Journal of Mechanics A/Solids 28, 752–756.
Lim, T.-C., Rajendra Acharya, U., 2011. Counterintuitive modulus from semi-auxetic laminates. Physica Status Solidi B 248 (1), 60–65.
Lira, C., Innocenti, P., Scarpa, F., 2010. Transverse elastic shear of auxetic multi re-entrant honeycombs. Composite Structures 90, 314–322.
Liu, Y., Hu, H., 2010. A review on auxetic structures and polymeric materials. Scientific Research and Essays 5 (10), 1052–1063.
Michelis, P., Spitas, V., 2010. Numerical and experimental analysis of a triangular auxetic core made of CFR-PEEK using the directionally reinforced integrated single-yarn (DIRIS) architecture. Composites Science and Technology 70, 1064–1071.
Miller, W., Hook, P.B., Smith, C.W., Wanga, X., Evans, K.E., 2009. The manufacture and characterisation of a novel, low modulus, negative Poisson's ratio composite. Composites Science and Technology 69, 651–655.
Miller, W., Smith, C.W., Evans, K.E., 2011. Honeycomb cores with enhanced buckling strength. Composite Structures 93, 1072–1077.
Narojczyk, J.W., Wojciechowski, K.W., 2008. Elastic properties of the fcc crystals of soft spheres with size dispersion at zero temperature. Physica Status Solidi B 245 (3), 606–613.
Narojczyk, J.W., Wojciechowski, K.W., 2010. Elastic properties of degenerate f.c.c. crystal of polydisperse soft dimers at zero temperature. Journal of Non-Crystalline Solids 356, 2026–2032.
Narojczyk, J.W., Alderson, A., Imre, A.R., Scarpa, F., Wojciechowski, K.W., 2008. Negative Poisson's ratio behavior in the planar model of asymmetric trimers at zero temperature. Journal of Non-Crystalline Solids 354, 4242–4248.
Nowacki, W., 1970. Theory of Micropolar Elasticity. Springer, Wien.
Pasternak, E., Dyskin, A.V., 2008a. Multiscale hybrid materials with negative Poisson's ratio. In: Borodich, F. (Ed.), IUTAM Symposium on Scaling in Solid Mechanics. Springer, pp. 49–58.
Pasternak, E., Dyskin, A.V., 2008b. Materials with Poisson's ratio near-1: properties and possible realisations, In: ICTAM 2008, Denier, J., Finn, M.D., Mattner T. (Eds.), XXII International Congress of Theoretical and Applied Mechanics, CD-ROM Proceedings ISBN 978-0-9805142-1-6, Paper 11982.
Pasternak, E., Dyskin, A.V., 2012. Materials and structures with macroscopic negative Poisson's ratio. International Journal of Engineering and Science 52, 103–114.
Pasternak, E., Mühlhaus, H.-B., 2001. Cosserat continuum modelling of granulate materials. In: Valliappan, S., Khalili, N. (Eds.), Computational Mechanics – New Frontiers for New Millennium. Elsevier Science, pp. 1189–1194.
Pasternak, E., Mühlhaus, H-B., 2005. Generalised homogenisation procedures for granular materials. Journal of Engineering Mathematics 52 (1–3), 199–229.
Pasternak, E., Mühlhaus, H-B., Dyskin, A.V., 2004. On the possibility of elastic strain localisation in a fault. Pure and Applied Geophysics 161 (11–12), 2309–2326.
Pasternak, E., Dyskin, A.V., Shufrin, I., 2010. Negative Poisson's ratio materials' design principles and possible applications. In: Proceedings of the 6th Australasian Congress on Applied Mechanics, ACAM 6, Kian Teh, Ian Davies, Ian Howard (Eds.), 12–15 December 2010, Perth, Paper 1266, p. 10.
Ravirala, N., Alderson, A., Alderson, K.L., 2007. Interlocking hexagons model for auxetic behaviour. Journal of Materials Science 42, 7433–7445.
Rothenburg, L., Berlin, A.A., Bathurst, R.J., 1991. Microstructure of isotropic materials with negative Poisson's ratio. Nature 354, 470–472.
Scarpa, F., Pastorino, P., Garelli, A., Patsias, S., Ruzzene, M., 2005. Auxetic compliant flexible PU foams: static and dynamic properties. Physica Status Solidi B 242 (3), 681–694.
Scarpa, F., Adhikari, S., Wang, C.Y., 2010. Nanocomposites with auxetic nanotubes. International Journal of Smart and Nano Materials 1 (2), 83–94.
Shokrieh, M.M., Assadi, A., 2011. Determination of maximum negative Poisson's ratio for laminated fiber composites. Physica Status Solidi B 248 (5), 1237–1241.
Shufrin, I., Pasternak, E., Dyskin, A.V., 2010. Symmetric structures with negative Poisson's ratio. In: Australian and New Zealand Industrial and Applied Mathematics Conference, ANZIAM – 2010, Queenstown, New Zealand.
Smith, C.W., Grima, J.N., Evans, K.E., 2000. A novel mechanism for generating auxetic behaviour in reticulated foams: missing rib foam model. Acta Materialia 48, 4349–4356.
Timoshenko, S.P., Goodier, J.N., 1982. Theory of Elasticity. McGraw-Hill book, Singapore.
Tretiakov, K.V., Wojciechowski, K.W., 2007. Poisson's ratio of simple planar 'isotropic' solids in two dimensions. Physica Status Solidi B 244 (3), 1038–1046.
Tshernykh, K.F., 1988. Introduction in Anisotropic Elasticity. Nauka, Moscow.
Vasiliev, A.A., Dmitriev, S.V., Ishibashi, Y., Shigenari, T., 2002. Elastic properties of a two-dimensional model of crystals containing particles with rotational degrees of freedom. Physical Review B 65, 094101.
Weaver, W., Gere, J.M., 1990. Matrix Analysis of Framed Structures, 3rd ed. Kluwer Academic Publishers, Netherlands.
Wei, G., Edwards, S.F., 1998. Poisson ratio in composites of auxetics. Physical Review E 58 (5), 6173–6181.
Williams, J.J., Smith, C.W., Evans, K.E., Lethbridge, Z.A.D., Walton, R.I., 2007. An analytical model for producing negative Poisson's ratios and its application in explaining off-axis elastic properties of the NAT-type zeolites. Acta Materialia 55, 5697–5707.
Wojciechowski, K.W., 1989. Two-dimensional isotropic system with a negative Poisson ratio. Physics Letters A 137 (1-2), 60–64.
Wojciechowski, K.W., 2003. Non-chiral, molecular model of negative Poisson' ratio in two dimensions. Journal of Physics A: Mathematical and General 36, 11765–11778.
Wright, J.R., Sloan, M.R., Evans, K.E., 2010. Tensile properties of helical auxetic structures: a numerical study. Journal of Applied Physics 108, 044905.
Yang, W., Li, Z.-M., Shi, W., Xie, B.-H., Yang, M.-B., 2004. Review on auxetic materials. Journal of Materials Science 39 (10), 3269–3279.
Zhang, R., Yeh, H.-L., Yeh, H.-Y., 1999. A discussion of negative Poisson's ratio design for composites. Journal of Reinforced Plastics and Composites 18, 1546–1556.